Ions generated from a premixed methane-air flame: mobility size distributions and charging characteristics

Chanakya Bagya Ramesh^{1,2}, Yang Wang^{1,2*}

¹ Department of Chemical, Environmental and Materials Engineering, University of Miami, Coral Gables, Florida, 33146, United States

² Department of Civil, Architectural and Environmental Engineering, Missouri University of Science and Technology, Rolla, Missouri, 65409, United States

Submitted to:

Combustion Science and Technology

* To whom correspondence should be addressed:

Tel: +1-305-284-3323

E-mail address: yangwang@miami.edu

Abstract

Chemical ionization in combustion systems forms concentrated ions of both polarities. Applying electric fields and plasmas to combustion systems has been shown to reduce emissions (such as particulate matter) potentially through controlling the ionic properties. Detailed flame-generated ion properties need to be characterized to better understand and predict the dynamics and roles of these ions in combustion and particle formation processes. In this work, we used a highresolution differential mobility analyzer (HR-DMA) to map the mobility and size distributions of positive and negative ions generated from a premixed methane-air flat flame under atmospheric pressure. Measurements were conducted over a wide range of stoichiometric ratios (0.8 to 1.2) and heights above the burner (HAB, 2 to 42 mm). Positively charged ions are relatively stable over the entire range of experimental conditions, showing two major modes, one at 1.17 and two overlapping modes at 1.38 and 1.53 nm. The ones corresponding to 1.38 and 1.53 nm showed gradual increase in size with HAB, indicating charging of hydrocarbon precursors. With the mobility values of the ions, we calculated their approximate mass values based on the empirical mobility-mass relationship and estimated the charging characteristics of particles in the flame. The ion profiles and particle charging characteristics obtained in this study will improve our understanding of the electrostatic interactions in flame systems.

1. Introduction

The precise control of particle formation during combustion is crucial for both the environmental applications of flame-synthesized particles (Gillon et al., 2019; Wang et al., 2017; Xiong et al., 2017) and the capture of combustion-generated hazardous particulate matter (Gillon et al., 2019; Michelsen, 2017). However, a detailed understanding of the particle dynamics in flames is lacking due to the strong involvement of flame-generated ions and the fast reaction rate of combustion. This knowledge gap leads to challenges in controlling the particle formation in combustion. Because of chemical ionization, flames generate large numbers of ions and charged clusters with concentrations as high as 10^{10} cm⁻³ (Fialkov, 1997). The highly concentrated ions and charged clusters actively collide with flame-generated particles, adding electrostatic potentials to the system, and altering the properties of the ions and particles (Vemury & Pratsinis, 1995; Wang et al., 2017). Recently, there has also been an increased interest in using external electric fields or plasmas to actively control combustion processes (Gillon et al., 2019; Xiong et al., 2017). These modified combustion systems have been shown to reduce emissions and improve combustion efficiency, showing that the ions in flames can play a significant role in affecting the combustion process and the downstream particle formation. However, due to instrument limitation, the ions and nascent particles generated during combustion still remain largely unmeasurable (Michelsen, 2017; Tang et al., 2017), and our understanding of the flamegenerated ion properties is still hindered by a lack of experimental data on the spatial distribution of ionic species in flames. Thus, experimental efforts towards a quantitative characterization of ions in flames are required.

Previous studies have been using the Langmuir probe to measure current signals generated under an electric field during combustion (Fialkov, 1997), so that the ion properties can be examined. The current and voltage can be used to derive the conductivity of the flame, which is further dependent on the concentration and electrical mobilities of the ions. This method also demonstrated its potential as a combustion diagnostic technique for engines and turbines (Dong et al., 2019). Although the Langmuir probe is very simple in design, it is relatively complex in theory, and the derivation of the ion concentrations relies on the assumptions of ion masses. The molecular beam mass spectrometry (MBMS) is another widely used instrument, which can provide the exact mass and compositions of the flame-generated ions (Hansen et al., 2009). Limited research on $CH_4 - O_2$ flames with the MBMS show that ion concentration profile depends significantly on the flame equivalence ratio (Goodings et al., 1979; Goodings et al., 1977), and in both lean and stoichiometric flames, $C_2H_3O^+$ and H_3O^+ were the most dominant positive ions. These studies also point out that with the introduction of N_2 , a strong NO^+ ion signal appear in the mass spectrum (Alquaity et al., 2017), and that the concentration of positive ions are generally higher than that of negative ions (Sugden et al., 1973), with electrons acting as the remaining negative charge carriers. Many of the MBMS studies on flame-generated ions were conducted at reduced pressure due to the challenge of sampling from the high temperature, where the ion chemistry may be affected due to the change of combustion conditions. Moreover have been relatively few detailed experimental studies on the examination of CH_4 -air flames, but given their prevalence in power generation and materials synthesis, the ion properties need to be investigated in such systems.

The movement of flame-generated ions is determined by their mobility and mass, where the direct measurement of such properties will benefit our understanding of their behaviors in flames. Previously, due to the high diffusivity of sub-3 nm particles and the limited instrument resolution, this type of measurement was challenging. High-resolution differential mobility analyzers (HR-DMAs) suppress particle diffusion and residence time in the instrument by using faster sheath flow and shortened instrument design, enabling the ion mobility measurement with significantly enhanced resolution (Fernández de la Mora & Kozlowski, 2013). The coupling of the HR-DMA with a mass spectrometer enables the simultaneous measurement of ion mobility and mass (Maißer et al., 2015), through which the accurate calculation of the interaction between ions and particles becomes possible (Reischl et al., 1996). Based on Fuchs' charging theory, the ion-particle combination coefficient is dependent on the mass and mobility of the ions (Fuchs, 1963). Fuchs' charging theory agrees reasonably well with the experimentally measured charging probabilities of particles between 3 nm and 1 µm, although it neglects the effect of particle surface and chemical properties (Wiedensohler & Fissan, 1991). By mapping the ion profiles in flames, we can examine the charging characteristics of particles formed in flames, through which the downstream particle growth and capture can be predicted.

In this work, we used the HR-DMA to measure the mobility and size distributions of positive and negative ions generated from a premixed methane-air flat flame under atmospheric pressure. Different stoichiometry ratios and heights above the burner (HAB) were applied to study the variation of ion profiles. Based on the empirical mobility-mass relationship, we estimated the mass values of these flame-generated ions and calculated the ion-particle combination coefficients and the charge fractions of flame-generated particles. This method can be applied to

combustion processes with modified ionic environments, where the particle charging characteristics can be predicted.

2. Methods

2.1. Experimental setup

Figure 1 shows the schematic diagram of the experimental setup. The system is composed of a premixed flat flame burner, a dilution sampling probe, a HR-DMA (Half-Mini type (Fernández de la Mora & Kozlowski, 2013), SEADM Inc.), and an aerosol electrometer (E12 Lynx, SEADM Inc.). A 60 mm-diameter premixed flat flame burner (Holthuis and Associates Inc.) was selected due to its uniformity and stability. The stainless steel sintered plug at the outlet of the burner creates a uniform velocity profile for combustion, and the flame is shielded with N_2 (Airgas Inc.) at a flow rate of 10 lpm. The gas mixture for combustion was composed of CH_4 (Airgas Inc.), O_2 (Airgas Inc.), and N_2 . Under the stoichiometric condition, the CH_4 , O_2 , and N_2 flow rates were maintained at 1, 2, and 7.52 lpm with mass flow controllers (Pneucleus Technologies LLC). Under the test condition of different stoichiometric ratios, the flow rates are adjusted accordingly while the flame front is maintained at around 7 mm above the burner. The flame temperature was measured with a type R thermocouple, and the temperature profile under stoichiometry is shown as the inset in Fig. 1. The temperature peaked at around 7 mm and gradually reduced at higher HABs. In the HAB range used in this study (7 to 42 mm), the temperature varied between 1400 and 1600 K.

Above the flame, a dilution sampling probe was used to withdraw the flame-generated ions to the downstream instruments while quenching further reactions and particle growth. The dilution

sampling probe is a hole-in-a-tube design (Zhao et al., 2003), where a 0.1 mm-diameter orifice at the bottom of the 1/4 inch stainless-steel tube withdrew charged particles from the flame. The dilution ratio (DR) is controlled by adjusting the pressure upstream and downstream of the orifice and is calculated considering thermal expansion in the flame (Zhao et al., 2003). Under the ambient temperature, a DR of 3800 can be achieved by comparing the concentrations of sampled particles before and after dilution. Our previous study shows that at DR above 160, the normalized size distributions of flame-generated sub-3 nm particles became asymptotic (Wang, 2017), suggesting that the dilution was sufficient to suppress the reaction and dynamics of the sampled species. Ionization sources were not applied in the system, meaning that the HR-DMA measured the natively charged ions only.

The HR-DMA was operated in a closed-loop so that the inlet and outlet sheath flows were balanced. The sheath flow was generated by a brushless blower (DOMEL Inc.), cooled by an inline homemade heat radiator, and cleaned by a high-efficiency particulate air (HEPA) filter (SEADM Inc.) before it entered the classification zone of the DMA. The DMA classifies and measures the electrical mobility of particles based on the balance between the drag force and the electrostatic force. When a voltage (V) is applied across the electrodes of the DMA, only particles with a certain electrical mobility (Z) can follow a specific trajectory to exit the classification zone of the DMA. The electrical mobility is correlated with the particle size by $Z = Cne/3\pi\mu D_{\rm p}$

where C is the Cunningham slip correction factor, n is the number of charges on the particle, e is the electronic charge, μ is the air viscosity, and D_p is the mobility size. Here, based on the previous measurements with the MBMS (Goodings et al., 1979; Goodings et al., 1977), we assume that the flame-generated ions carry one charge only. The classified ions with the same electrical mobility were be introduced to the electrometer, and the concentration of the ions (N) is determined by the current (I) measured electrometer and the dilution ratio, where $N = DR \times I/eQ_a$. Here, Q_a is the flow rate through the electrometer, which was maintained by a critical orifice at 6.08 lpm. In order to calculate the charging characteristics of the flame-generated ions, the mass of the ions also needs to be obtained. In this study, we applied the mass-mobility relationship presented by Kilpatrick (Mäkelä et al., 1996) to convert the electrical mobility into mass (m) using

$$Z = \exp \left[-0.0347 ln^2(m) - 0.0376 ln(m) + 1.14662 \right]$$
 (2) where Z and m carry the units of cm² V⁻¹ s⁻¹ and Da.

The voltage across the DMA was applied by a high voltage power supply (Bertan 205B, Spellman Inc.). The voltage applied onto the DMA and the current registered by the electrometer were controlled and recorded by a data acquisition system (Model 6008, National Instruments Corp). It should be noted that the mobility size does not necessarily represent the ion physical size, since the chemical composition of the ions determines the structure of the cluster, while the size of these non-spherical clusters is challenging to be properly defined. Existing studies show that the volumetric size of sub-3 nm particles generally agrees well with the mobility size of the particle subtracted by 0.3 nm (Larriba et al., 2011). However, for simplicity, we reported the concentrations based on the mobility size and the electrical mobility of the particles. The HR-

DMA was calibrated with the organic ions generated by electro-spraying a 0.2 mM tetraheptylammonium bromide-methanol solution to ensure its sizing accuracy (Ude & De La Mora, 2005).

Two sets of experiments were conducted to map the mobility size distributions of ions generated from the flame. The first set of experiments examined the effect of equivalence ratio (ϕ = 0.8, 0.9, 1.0, 1.1, and 1.2) on the positive and negative ion size distribution, while the second set of experiments studied the effects of sampling HAB (HAB = 7, 12, 17, 22, 32, and 42 mm). In the first set of experiments, HAB was fixed at 7 mm, and in the second set, ϕ was fixed at 1.0.

2.2 Calculation of particle charging dynamics

Due to chemical ionization, the flame acts as a quasi-neutral plasma that generates high concentrations of ions. These ions are able to charge the nascent particles, such as soot or synthesized nanoparticles. The charging process is strongly dependent on the ion-particle combination coefficient, which can be calculated based on the mobility and mass of the ions. According to Fuchs' charging theory (Fuchs, 1963; Reischl et al., 1996), the ion-particle combination coefficient (η_i^{\pm}) of positive (+) or negative (-) ions with a particle carrying i elementary charges can be derived as

$$\eta_{i}^{\pm} = \frac{\beta_{i}^{\pm} \exp[-\phi_{i}(\delta^{\pm})/kT]}{\left[1 + \exp[-\phi_{i}(\delta^{\pm})/kT]\left[\beta_{i}^{\pm}/4\pi D^{\pm}\right] \times \int_{0}^{1} \exp[-\phi_{i}(\delta^{\pm}/x)/kT]dx\right]}$$
(3)

In this equation, β_i^{\pm} is the proportionality between the ion flux onto a particle and the ion concentration, δ^{\pm} is the radius of the limiting sphere (inside which the movement of ions is guided by the electrostatic potential between the ion and the particle), ϕ_i is the electrostatic

potential energy of the ion in the field of the particle, k is the Boltzmann's constant, T is temperature, and D^{\pm} is the diffusion coefficient of the ions. ϕ_i and δ^{\pm} are calculated by

$$\phi_i(r) = \frac{e^2}{4\pi\varepsilon_0} \left\{ \frac{i}{r} - K \frac{r_p^3}{2r^2[r^2 - r_p^2]} \right\}$$
(4)

$$\delta^{\pm} = \frac{r_p^3}{\lambda^{\pm 2}} \left[\frac{1}{5} \left(1 + \frac{\lambda^{\pm}}{r_p} \right)^5 - \frac{1}{3} \left(1 + \frac{\lambda^{\pm 2}}{r_p^2} \right) \left(1 + \frac{\lambda^{\pm}}{r_p} \right)^3 + \frac{2}{15} \left(1 + \frac{\lambda^{\pm 2}}{r_p^2} \right)^{5/2} \right] (5)$$

where r is any location outside the particle, ε_o is the dielectric constant of the vacuum, K is the conductivity of the particle (K= 1 in this study, assuming that), r_p is the radius of the particle, and λ^{\pm} is the mean free path of the positive or negative ions. λ^{\pm} , D^{\pm} and β_i^{\pm} are functions of ion mass and mobility, following the relationships of

$$\lambda^{\pm} = \frac{32}{3\pi} \frac{D^{\pm}}{\bar{c}^{\pm}} \frac{M}{M + m^{\pm}} \tag{6}$$

$$D^{\pm} = kTZ^{\pm}/e \tag{7}$$

$$\beta_i^{\pm} = \pi (\delta^{\pm})^2 \bar{c}^{\pm} \alpha_i^{\pm} \quad (8)$$

where Z^{\pm} is the electrical mobility of the positive or negative ions, \bar{c} is the mean thermal velocity of the ions $(\bar{c} = (8kT/\pi m^{\pm})^{1/2})$, m^{\pm} is the mass of the positive or negative ions, M is the mass of the air molecules, and α_i^{\pm} is the collision probability between the positive or negative ions with the particle carrying i elementary charges within the limiting sphere (Reischl et al., 1996).

With η_i^{\pm} , we can calculate the fraction of particles carrying p number of positive or negative charges among all particles of the same size (f_p^{\pm}) , where

$$f_p^{\pm} = \frac{N_p^{\pm}}{N} = \frac{\prod_{j=1}^p A_j^{\pm}}{\left[1 + \sum_{k=1}^m \left(\prod_{j=1}^k A_j^{-} + \prod_{j=1}^k A_j^{+}\right)\right]}$$
(9)

Here, m is the maximum number of charges carried by the particle (assumed to be 30 in this study). A_j^{\pm} is the concentration ratio between particles carrying j and j-1 charges, and is calculated by

$$A_{j}^{\pm} = \frac{n^{\pm}}{n^{\mp}} \frac{\eta_{2_{j-1}}^{\pm}}{\eta_{1_{j}}^{\mp} + \eta_{2_{j}}^{\pm} n^{\pm} / n^{\mp} - \eta_{1_{j+1}}^{\mp} A_{j+1}^{\pm}}$$
(10)

 n^{\pm} is the concentration of positive or negative ions (assumed to be equal in this study). $\eta 1_p^{\mp}$ is the ion-particle combination coefficient between ions and particles carrying p charges of the opposite sign as the ions, and $\eta 2_p^{\pm}$ is that of the same sign as the ions.

The mobilities measured by the HR-DMA and the approximate masses based on Eq. (2) were used as inputs for calculating η_i^{\pm} and f_p^{\pm} . The DMA-measured mobilities at 298 K were converted to those under flame temperature (1600 K) by assuming that the mobility of the particle in the free molecular regime is proportional to $T^{0.5}$ (Larriba et al., 2011). A detailed derivation of the terms in Eq. (3) can be found elsewhere (Reischl et al., 1996).

3. Results and Discussion

3.1. Mobility size distributions of ions generated from flames

The mobility size distributions of positive and negative ions sampled at the equivalence ratio of 1.0 and a HAB of 7 mm are shown in Fig. 2. Both types of ions show two kinds of peaks. First is a highly resolved peak at smaller size. Second is a much broader peak at a bigger size. The highly resolved peak indicates that ionic species with stable chemical compositions are formed from combustion. Whereas the broader peak is likely a result of these ions interacting with other molecules, resulting in larger charged clusters.

The positive ions have a relatively narrow peak at size 1.17 nm, and two broader overlapping peaks at sizes 1.38 nm and 1.53 nm. The negative ions also have a narrow peak and two broad overlapping peaks. The narrow peak is at the size 1.01 nm and the two broader overlapping peaks are at the sizes 1.19 nm and 1.32 nm. The corresponding mobilities for these ions are 1.51, 1.09, and 0.89 cm² V⁻¹ s⁻¹ for the positive ions, and 2.03, 1.46, and 1.19 cm² V⁻¹ s⁻¹ for the negative ions. According to Eq. (3), their approximate mass values are 148, 326, and 510 Da for positive ions; and 64, 161, and 266 Da for negative ions. These ions are most likely generated because of chemical ionization rather than thermal ionization, because the relatively low temperature of the flame (below 2200 K) would result in an approximate thermally ionized ion concentration below 10⁻¹² cm⁻³ (Calcote, 1957).

According to recent work with MBMS, the dominant positive ions in fuel rich methane-oxygen flames are $C_3H_3^+$, $C_2H_3O^+$, and H_3O^+ (Jones & Hayhurst, 2016). For fuel-lean conditions, CH_5O^+ , $C_2H_3O^+$ and H_3O^+ . And for stochiometric conditions, $C_2H_3O^+$ and H_3O^+ (Alquaity et al., 2017). These positive ions can actively collide with other molecules to form more stable ions. One can notice that the sizes of the HR-DMA-measured ions are larger than the values expected for a cluster composed of a few atoms. According to molecular dynamics simulations, the mobility size of a charged particle is inherently larger than its volumetric size. Our previous studies combining the HR-DMA with a mass spectrometer show that the major negative ionic peak at 1.01 nm is NO_3^- (Wang et al., 2017), which has a thermochemical ionic radius of 0.179 nm (Jenkins & Thakur, 1979). Note that NO_3^- has a molecular mass of 62 Da, which is very close to the value predicted by Eq. (2) (61 Da). It is also possible that the cooling of the sampled

ions led to the transformation of their chemical composition, which could occur even before they were withdrawn by the sampling probe. The use of metallic dilution sampling probe could further affect the ions by creating a temperature gradient around its inlet (Knyazkov et al., 2022; Lupant et al., 2010). The average mobility of negative ions was higher than that of positive ions, potentially because the positive ions were composed of organic species, which had higher proton affinities.

From the size distributions, we can also observe that the concentration of the positive ions is higher than that of the negative ions, with a concentration ratio of 2.2:1. This is mainly because electrons are an important negative charge carrier in flames, and they cannot be detected due to their small size. A previous study on the methane-oxygen flame observed that the concentrations of positive and negative ions are 4×10^{10} and 1.5×10^{10} cm⁻³ (Sugden et al., 1973), respectively. The significant lower concentrations of the ions measured by the HR-DMA (in the order of 10^5 cm⁻³) is likely due to the sampling loss and the low transmission efficiency of the ions through the instrument (Kangasluoma et al., 2016). According to Fuchs charging theory (Eqs. (3) to (10)), the absolute concentrations of the ions do not affect the calculation of the particle charging characteristics, and therefore, ion size and mobility in the measured size distributions can be used to estimate their charging characteristics. To more accurately measure the total ion concentrations in flames, a Langmuir probe should be used.

3.2. Influence of flame equivalence ratio and sampling height

The effect of flame equivalence ratio (ϕ) on the size distributions of the flame-generated ions at the HAB of 7 mm is shown in Fig. 3. As we change ϕ from 0.8 to 1.2, we can see that the flame

structure changes from a flat structure to a more conical structure due to the faster heat dissipation and therefore the slower reaction rate at the outer region of the flame (Fig. 4). So, depending on the equivalence ratio of the flame, for the same sampling height, ions from different regions of the flame were sampled. For ϕ values of 0.8, 1.0, and 1.2, for a sampling height of 7 mm, ions were studied from the trailing region, flame front, and from within the flame. At $\phi = 1.2$, most positive ions have a mobility diameter of 1.17 nm (Fig. 3a). As we move towards the lower ϕ , we notice that the concentration of ions corresponding to diameter 1.17 nm decreases and there is an emergence of two overlapping secondary peaks at 1.38 nm and 1.53 nm. For negative ions, we see similar primary and two overlapping secondary peaks. The primary peak is dominated by ions with a mobility diameter of 1.01 nm, and the secondary peaks are dominated by ions with a mobility diameter of 1.19 nm and 1.32 nm.

For the ϕ values tested, we see that the primary peaks for both positive and negative ions at 1.17 nm and 1.01 nm remain stable. The secondary peak starts emerging with decreasing ϕ value. This is when the flame structure changes from a conical to a flatter flame and we start looking at ions from the flame front to the trailing regions of the flame. The higher concentrations at lower ϕ suggests the charging of hydrocarbon precursors in the trailing region by positive and negative ions with mobility diameters of 1.17 nm and 1.01 nm. By summing the concentration of ions detected at each specific size, we also calculated the approximate total concentration of ions over the entire size range (Fig. 3), which is represented in terms of arbitrary units. Note that rigorously speaking, the total concentration needs to be calculated using the transfer function, ion transmission efficiency, and charging probability of the ions (Wang et al., 2014), which are challenging to obtain. Here, the approximate total concentration qualitatively shows that both the

positive and negative ion concentrations increased with ϕ , and the increase for positive ion concentration is more significant.

The influence of sampling HAB on the size distributions of the flame-generated ions at $\phi = 1.0$ is displayed in Fig. 5a and Fig. 5b. The size corresponding to the primary peak for positive ions remains relatively constant over range of sampling heights considered, indicating that there is minimal chemical transformation of these ions downstream of the flame. The concentration of positive ions at HAB = 42 mm is approximately 50% of that at HAB = 7 mm and the concentration of negative ions at HAB = 42 mm is approximately 65% of that at HAB = 7 mm. But when we look at the secondary peak of positive ions, we see that they are not as stable as the primary peak. As HAB increases, the secondary peak shifts towards a larger mobility diameter of around 1.5 nm with a mobility of 0.91 cm² V⁻¹ s⁻¹. This is an indicator of the growth of these charged hydrocarbon clusters which tend to act as precursors, which in turn initiate particle formation and their growth. Within the flame, positive ions have mobility diameter of 1.17 nm with a mobility of 1.52 cm² V⁻¹ s⁻¹. Negative ions have mobility diameter of 1.01 nm with a mobility of 2.13 cm² V⁻¹ s⁻¹. The higher fraction of positive ions than negative ions is likely because the remaining negative charge carriers in the flame are electrons, which have higher mobility than the measured negative ions within the flame. As electrons have a size which is smaller than the half-mini DMA's observable size range, we could not measure them. The presence of such high mobility ions of both polarities along with electrons will affect the particle charging in flames.

3.3. Particle charging in flames

With the mobility and mass of the positive and negative ions generated from the flame, we can use Fuchs' model Eqs. (3) to (10) to estimate the charging characteristics of particles in flames. Since multiple ions in the same polarity were detected, we first analyzed the sensitivity of ion-particle combination coefficients (η_i^{\pm}) to the mobility of the ions. Figure 6 shows the η_i^{\pm} as a function of particle size, where the particles may carry 0, +1, or -1 charges and the ions may be positive or negative ions. Note that Fig. 6a shows the calculated η_i^{\pm} using positive and negative ion mobilities of 1.52 and 2.13 cm² V⁻¹ s⁻¹ (peaks corresponding to 1.17 and 1.01 nm in Fig. 2), and Fig. 6b shows the calculated η_i^{\pm} using positive and negative ion mobilities of 0.92 and 1.12 cm² V⁻¹ s⁻¹. Using different sets of ion mobilities can lead to 2 to 4 times of difference in η_i^{\pm} , and the more mobile ions have a higher ion-particle combination rate. Therefore, the accurate determination of η_i^{\pm} in flames relies on the accurate measurement of ion mobility and mass in flames.

Given the higher mobility and smaller mass of the negative ions, η_i^{\pm} for negative ions is around 2 times of that of positive ions, meaning that particles have a higher probability of carrying negative ions. The higher negative charge fraction is observed in multiple previous studies on particle charge fraction in flames (Kim et al., 2005; Sahu et al., 2012). Apart from the negative ions, electrons are also an important negative charge carrier in flames, and they will participate in the particle charging process. A simulation study showed that the mobility of electrons in flames is largely independent of equivalence ratio and approximately equal to 400 cm² V⁻¹ s⁻¹ (Bisetti & El Morsli, 2012), which is significantly larger than those of ions. Therefore, the particles in flames may be dominantly in the negative charging state. As particle size increases, η_i^{\pm} also increases due to the larger collision area of the particles. For neutral particles, η_i^{\pm}

increases by almost 3 orders of magnitudes, from 10^{-14} to 10^{-11} m³ s⁻¹ as particle size increases from 1 to 100 nm. When the particle and ion carry the same type of charges, the repulsion between the particle and ion leads to a significantly lower η_i^{\pm} , compared to the cases of neutral particles and the particle and ion carrying opposite charges, especially when particles are below 10 nm. However, when particle sizes are close or above 100 nm, the repulsion or attraction between the particle and ion becomes less influential, and η_i^{\pm} converges to similar values for different charging states of the particles. This convergence of η_i^{\pm} also means that particles will carry multiple elementary charges at larger sizes. However, ion mobility and mass still play an important role at larger particle size, and larger particles have a propensity of carrying negative charges.

The charge fraction of particles in flames can be calculated based on Eq. (9), and the results are shown in Fig. 7. Weight-averaged ion mobility values based on the size distributions of the flame-generated ions (Fig. 2) are used, yielding positive and negative ion mobilities of 1.12 and 1.99 cm² V⁻¹ s⁻¹. To examine the influence of temperature on particle charging, we simulated the charge fraction under 1600 K (Fig. 7a) and 298 K (Fig. 7b). The fraction of neutral particles under 1600 K is significantly lower than that of 298 K, showing that the higher temperature can expedite the charging of particles in flames. The fractions of particles carrying one and two charges at 1600 K are also higher than those at 298 K. As particle sizes increase, the fractions of particles carrying one or two charges first increase, and then decrease. This decrease of the charge fraction was due to more particles carrying more than two elementary charges as particle size increases. Overall, the charge fraction of particles under flame temperature is much higher than that of ambient conditions.

Studying the flame-generated particle dynamics requires not only the accurate prediction of the particle charging process, but also a sufficient understanding of the particle-particle interactions, such as coagulation, sintering, and aggregation (Tsantilis et al., 2002). Our previous study simulating the simultaneous charging and coagulation of flame-generated particles shows that particle charging dominates the particle dynamics when the total concentration of ions is higher than that of particles (Wang et al., 2017). The addition of electric fields and plasmas in flames will affect the dynamics of ion-particle and particle-particle interactions, affecting the flame-generated particles. This study shows that the information of the ion properties in flames can be used to predict the charging characteristics of particles and their downstream formation.

4. Conclusion

In this work, we used a high-resolution differential mobility analyzer (HR-DMA) system to investigate the size distribution of ions generated in a premixed methane-air flame. The measurements were conducted over a range of stochiometric ratios and HABs. The positive ions generated from flames are relatively stable and showed a narrow peak at 1.17 nm and broader peaks at 1.38 and 1.53 nm. The concentration of 1.38 and 1.53 nm ions is higher for fuel-lean conditions where the sampling is done in the trailing regions of the flame. This indicates the charging of hydrocarbon precursors. The positive ion concentrations decreased gradually with HAB. While the primary peak of positive ions remained relatively stable, the secondary peak shifted slightly towards the larger diameter with increasing HAB, indicating the growth of hydrocarbon clusters. The estimation of the charging characteristics of particles shows that ion

mobilities can affect the ion-particle combination coefficient, and the high temperature of the flame can significantly increase the charge fraction of particles during combustion.

References

- Alquaity, A. B. S., Han, J., Chahine, M., Selim, H., Belhi, M., Sarathy, S. M., Bisetti, F., & Farooq, A. (2017). Measurements of Positively Charged Ions in Premixed Methane-Oxygen Atmospheric Flames. *Combustion Science and Technology*, 189(4), 575–594.
- Bisetti, F., & El Morsli, M. (2012). Calculation and analysis of the mobility and diffusion coefficient of thermal electrons in methane/air premixed flames. *Combustion and Flame*, *159*(12), 3518–3521.
- Calcote, H. F. (1957). Mechanisms for the formation of ions in flames. *Combustion and Flame*, *1*(4), 385–403.
- Dong, G., Lu, H., Wu, Z., Dibble, R., & Li, L. (2019). Effect of electric fields on the ion current signals in a constant volume combustion chamber. *Proceedings of the Combustion Institute*, 37(4), 4865–4873.
- Fernández de la Mora, J., & Kozlowski, J. (2013). Hand-held differential mobility analyzers of high resolution for 1-30nm particles: Design and fabrication considerations. *Journal of Aerosol Science*, 57, 45–53.
- Fialkov, A. B. (1997). Investigations on ions in flames. *Progress in Energy and Combustion Science*, 23(5–6), 399–528.
- Fuchs, N. A. (1963). On the stationary charge distribution on aerosol particles in a bipolar ionic atmosphere. *Geofisica Pura e Applicata*, *56*(1), 185–193.
- Gillon, P., Gilard, V., Idir, M., & Sarh, B. (2019). Electric field influence on the stability and the soot particles emission of a laminar diffusion flame. *Combustion Science and Technology*, 191(2), 325–338.

- J. Goodings, D. Bohme, T. Sugden, in: Symposium (International) on Combustion, Elsevier, 1977, pp. 891-902
- Goodings, J. M., Bohme, D. K., & Ng, C. W. (1979). Detailed ion chemistry in methaneoxygen flames. I. Positive ions. *Combustion and Flame*, *36*(C), 27–43.
- Hansen, N., Cool, T. A., Westmoreland, P. R., & Kohse-Höinghaus, K. (2009). Recent contributions of flame-sampling molecular-beam mass spectrometry to a fundamental understanding of combustion chemistry. *Progress in Energy and Combustion Science*, 35(2), 168–191.
- Jenkins, H. D. B., & Thakur, K. P. (1979). Reappraisal of thermochemical radii for complex ions. *Journal of Chemical Education*, 56(9), 576–577.
- Jones, H. R. N., & Hayhurst, A. N. (2016). Measurements of the concentrations of positive and negative ions along premixed fuel-rich flames of methane and oxygen. *Combustion and Flame*, 166, 86–97.
- Kangasluoma, J., Attoui, M., Korhonen, F., Ahonen, L., Siivola, E., & Petäjä, T. (2016).

 Characterization of a Herrmann-type high-resolution differential mobility analyzer. *Aerosol Science and Technology*, 50(3), 222–229.
- Kim, S. H., Woo, K. S., Liu, B. Y. H., & Zachariah, M. R. (2005). Method of measuring charge distribution of nanosized aerosols. *Journal of Colloid and Interface Science*, 282(1), 46–57.
- Knyazkov, D. A., Gerasimov, I. E., Bolshova, T. A., Kiselev, V. G., Shmakov, A. G., & Paletsky, A. A. (2022). Cationic structure of premixed near-stoichiometric CH4/O2/Ar flames at atmospheric pressure: New insights from mass spectrometry, quantum chemistry, and kinetic modeling. *Combustion and Flame*, 241.

- Larriba, C., Hogan, C. J., Attoui, M., Borrajo, R., Garcia, J. F., & De La Mora, J. F. (2011). The mobility-volume relationship below 3.0 nm examined by tandem mobility-mass measurement. *Aerosol Science and Technology*, 45(4), 453–467.
- Lupant, D., Pesenti, B., & Lybaert, P. (2010). Influence of probe sampling on reacting species measurement in diluted combustion. *Experimental Thermal and Fluid Science*, *34*(5), 516–522.
- Maißer, A., Thomas, J. M., Larriba-Andaluz, C., He, S., & Hogan, C. J. (2015). The mass-mobility distributions of ions produced by a Po-210 source in air. *Journal of Aerosol Science*, 90, 36–50.
- Mäkelä, J. M., Jokinen, V., Mattila, T., Ukkonen, A., & Keskinen, J. (1996). Mobility distribution of acetone cluster ions. *Journal of Aerosol Science*, *27*(2), 175–190.
- Michelsen, H. A. (2017). Probing soot formation, chemical and physical evolution, and oxidation: A review of in situ diagnostic techniques and needs. *Proceedings of the Combustion Institute*, *36*(1), 717–735.
- Reischl, G. P., Mäkelä, J. M., Karch, R., & Necid, J. (1996). Bipolar charging of ultrafine particles in the size range below 10 nm. *Journal of Aerosol Science*, 27(6), 931–949.
- Sahu, M., Park, J., & Biswas, P. (2012). In situ charge characterization of TiO 2 and Cu-TiO 2 nanoparticles in a flame aerosol reactor. *Journal of Nanoparticle Research*, 14(2).
- T. Sugden, J. Goodings, J. Jones, D. Parkes, Combustion Institute European Symposium, (1973) 250-255
- Tang, Q., Cai, R., You, X., & Jiang, J. (2017). Nascent soot particle size distributions down to 1 nm from a laminar premixed burner-stabilized stagnation ethylene flame. *Proceedings of the Combustion Institute*, *36*(1), 993–1000.

- Tsantilis, S., Kammler, H. K., & Pratsinis, S. E. (2002). Population balance modeling of flame synthesis of titania nanoparticles. *Chemical Engineering Science*, *57*(12), 2139–2156.
- Ude, S., & De La Mora, J. F. (2005). Molecular monodisperse mobility and mass standards from electrosprays of tetra-alkyl ammonium halides. *Journal of Aerosol Science*,
- Vemury, S., & Pratsinis, S. E. (1995). Corona-assisted flame synthesis of ultrafine titania particles. *Applied Physics Letters*, *66*(1995), 2424.
- Y. Wang, Sub 2 nm particle characterization in systems with aerosol formation and growth, Washington University in St. Louis, 2017.
- Wang, Y., Fang, J., Attoui, M., Chadha, T. S., Wang, W.-N., & Biswas, P. (2014). Application of Half Mini DMA for sub 2nm particle size distribution measurement in an electrospray and a flame aerosol reactor. *Journal of Aerosol Science*, 71, 52–64.
- Wang, Y., Kangasluoma, J., Attoui, M., Fang, J., Junninen, H., Kulmala, M., Petäjä, T., & Biswas, P. (2017). Observation of incipient particle formation during flame synthesis by tandem differential mobility analysis-mass spectrometry (DMA-MS). *Proceedings of the Combustion Institute*, 36(1), 745–752.
- Wang, Y., Sharma, G., Koh, C., Kumar, V., Chakrabarty, R., & Biswas, P. (2017). Influence of flame-generated ions on the simultaneous charging and coagulation of nanoparticles during combustion. *Aerosol Science and Technology*, 51(7), 833–844
- Wiedensohler, A., & Fissan, H. J. (1991). Bipolar charge distributions of aerosol particles in high-purity argon and nitrogen. *Aerosol Science and Technology*, *14*(3), 358–364.
- Xiong, G., Kulkarni, A., Dong, Z., Li, S., & Tse, S. D. (2017). Electric-field-assisted stagnation-swirl-flame synthesis of porous nanostructured titanium-dioxide films. *Proceedings of the Combustion Institute*, *36*(1), 1065–1075.

Zhao, B., Yang, Z., Wang, J., Johnston, M. V., & Wang, H. (2003). Analysis of soot nanoparticles in a laminar premixed ethylene flame by scanning mobility particle sizer.

Aerosol Science and Technology, 37(8), 611–620.

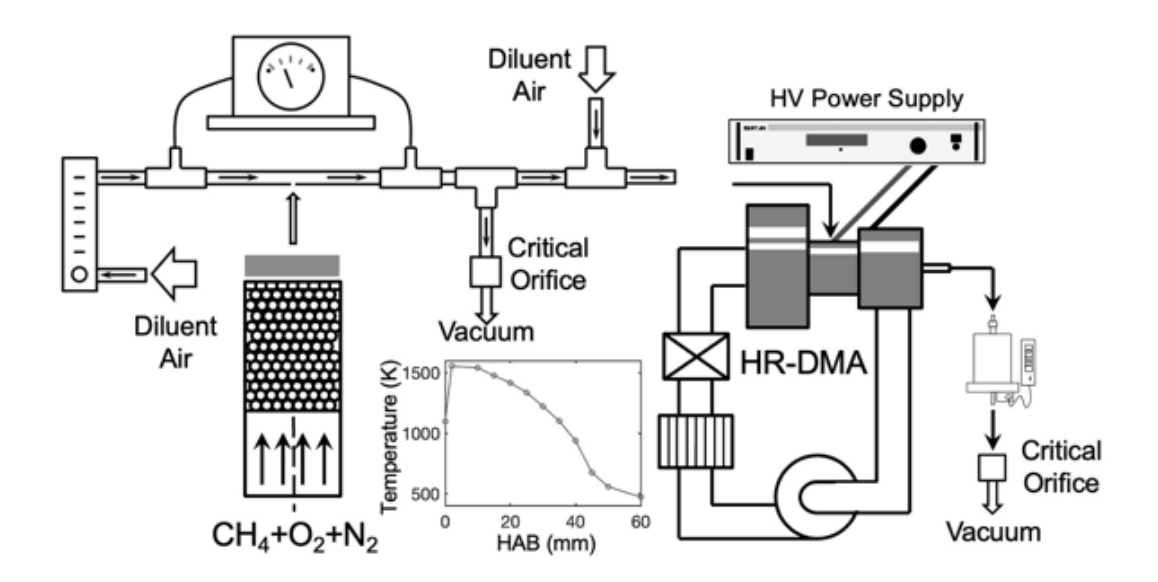


Fig 1. Schematic diagram of the experimental setup. The inset figure shows the temperatures measured at different heights above the burner.

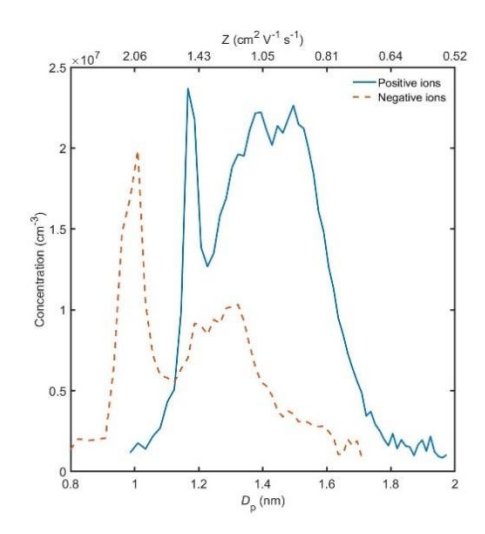


Fig 2. Size distributions of the positive and negative ions measured by the HR-DMA. The lower and upper x-axes show the mobility size and mobility of the ions.

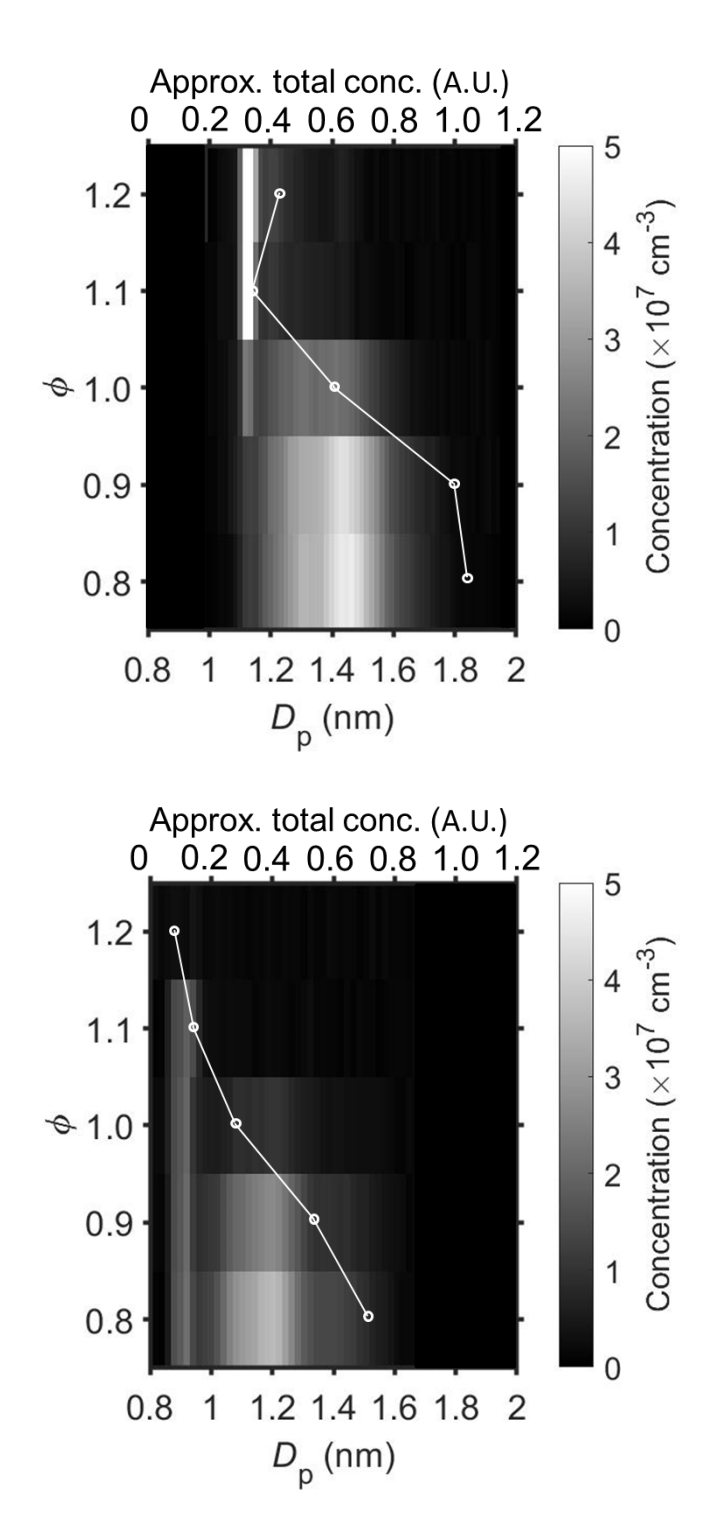


Fig. 3. Mobility size distribution of (a) positive and (b) negative ions under equivalence ratio (ϕ) of 0.8, 0.9, 1.0, 1.1, and 1.2. Line plots represent the approximate total concentration of the ions.

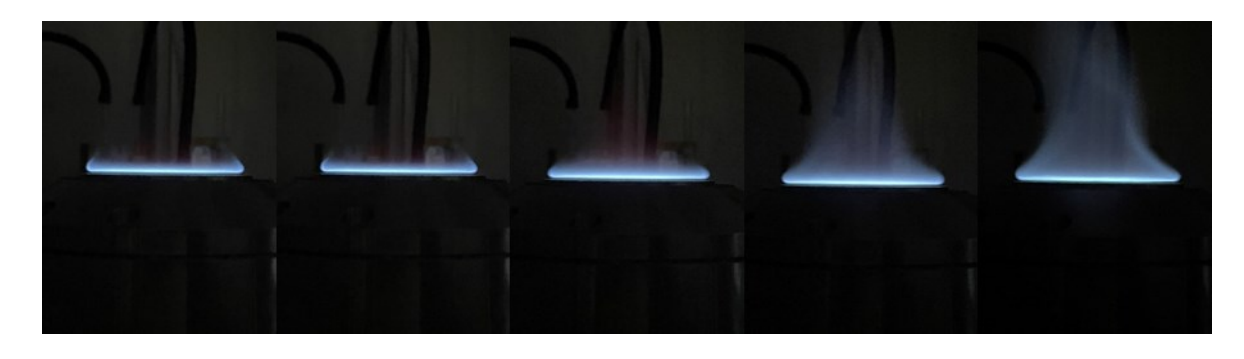


Fig. 4. Variation of flame structure with ϕ . From left to right, $\phi = 0.8, 0.9, 1.0, 1.1,$ and 1.2

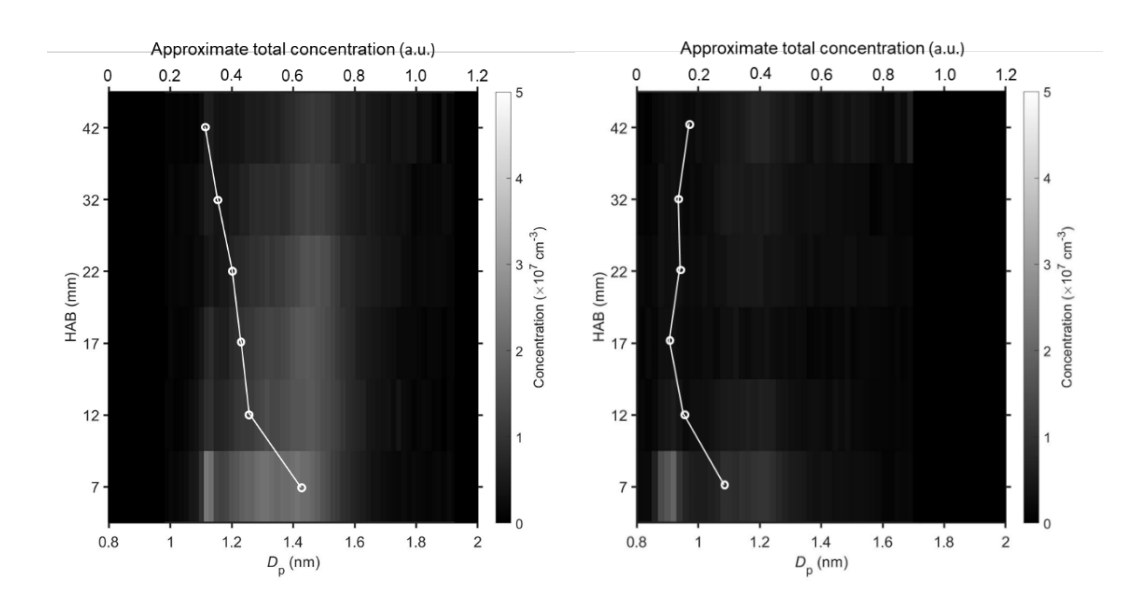


Fig. 5. Mobility size distributions of (a) positive and (b) negative ions measured at HAB of 7, 12, 17, 22, 32 and 42 mm. Line plots represent the approximate total ion concentration.

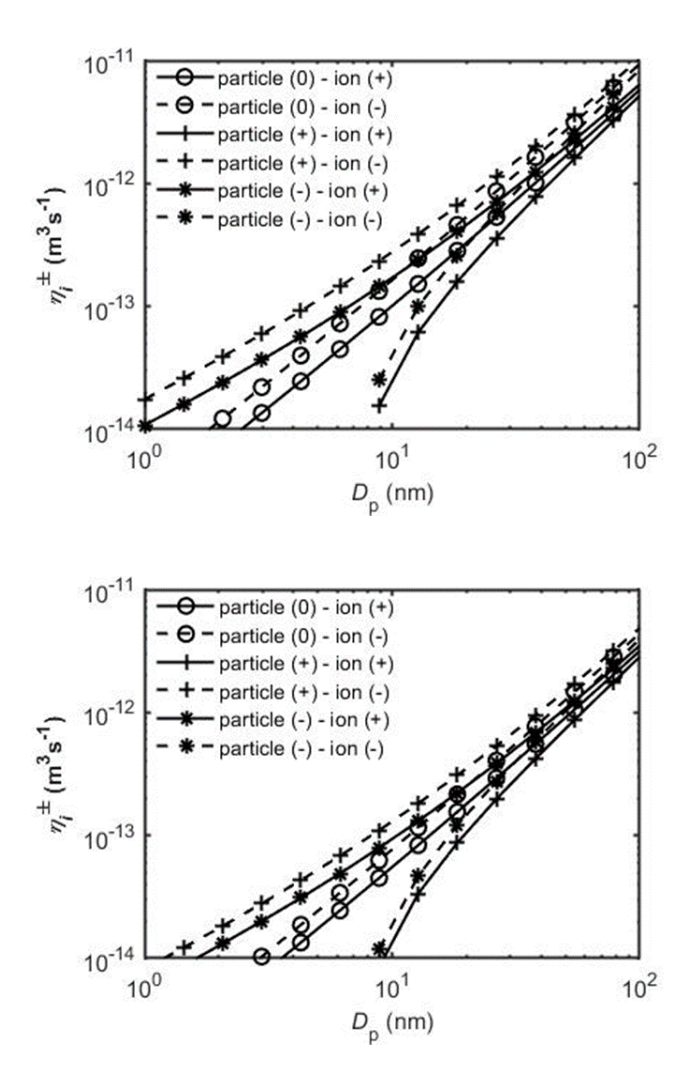


Fig. 6. Ion-particle combination coefficient (η_i^{\pm}) calculated using (a) positive and negative ion mobilities of 1.52 and 2.13 cm² V⁻¹ s⁻¹ and (b) positive and negative ion mobilities of 0.91 and 1.12 cm² V⁻¹ s⁻¹. Labels of "particle (0)", "particle (+)", and "particle (-)" indicate particles are neutral, carrying one positive elementary charge, and carrying one negative elementary charge, respectively. Labels of "ion (+)" and "ion (-)" indicate ions are carrying one positive elementary charge and one negative elementary charge, respectively.

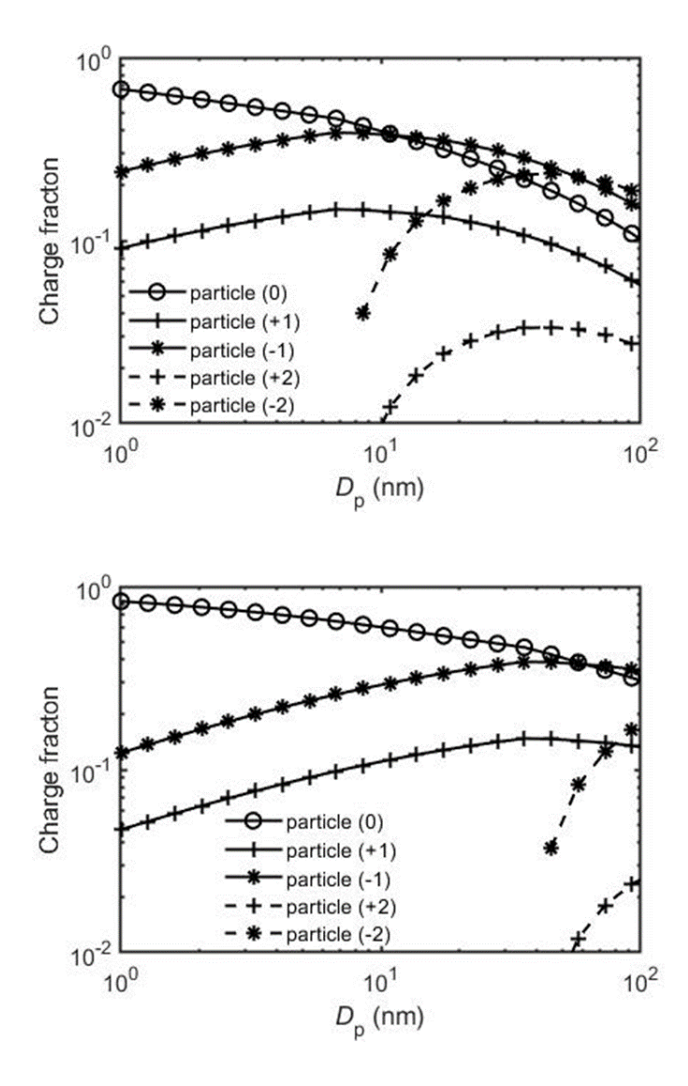


Fig. 7. Charge fraction of particles simulated under temperatures of (a) 1600 K and (b) 298 K. Labels of "(0)", "(+1)", "(+2)", "(-1)", and "(-2)" indicate particles are neutral, carrying one positive, two positive, one negative and two negative elementary charges, respectively.